

Active and passive shielding design optimization and technical solutions for deep sensitivity hard X-ray focusing telescopes

G. Malaguti^a, G. Pareschi^b, P. Ferrando^c, E. Caroli^a, G. Di Cocco^a, L. Foschini^a, S. Basso^b, S. Del Sordo^d, F. Fiore^e, A. Bonati^f, G. Lesci^f, J.M. Poulsen^f, F. Monzani^f, A. Stevoli^f, B. Negri^g

^a INAF, Istituto di Astrofisica Spaziale e Fisica Cosmica, Sezione di Bologna, via P. Gobetti 101, 40129 Bologna, Italy

^b INAF, Osservatorio Astronomico di Brera, via E. Bianchi 46, 23807 Merate Italy

^c DSM/DAPNIA/Service d'Astrophysique, CEA/Saclay, 91191 Gif-sur-Yvette Cedex, France

^d INAF, Istituto di Astrofisica Spaziale e Fisica Cosmica, Sezione di Palermo, via La Malfa 153, 90146 Palermo, Italy

^e INAF, Osservatorio Astronomico di Roma, via Frascati 33, 00040 Monteporzio, Italy

^f Alenia Spazio SpA LABEN, Strada Padana Superiore 290, 20090 Vimodrone, Italy

^g ASI, Agenzia Spaziale Italiana, Viale Liegi 26, 00198 Roma, Italy

ABSTRACT

The 10–100 keV region of the electromagnetic spectrum contains the potential for a dramatic improvement in our understanding of a number of key problems in high energy astrophysics. A deep inspection of the universe in this band is on the other hand still lacking because of the demanding sensitivity (fraction of μCrab in the 20–40 keV for 1 Ms integration time) and imaging ($\approx 15''$ angular resolution) requirements. The mission ideas currently being proposed are based on long focal length, grazing incidence, multi-layer optics, coupled with focal plane detectors with few hundreds μm spatial resolution capability. The required large focal lengths, ranging between 8 and 50 m, can be realized by means of extendable optical benches (as foreseen e.g. for the HEXIT-SAT, NEXT and NuSTAR missions) or formation flight scenarios (e.g. Simbol-X and XEUS). While the final telescope design will require a detailed trade-off analysis between all the relevant parameters (focal length, plate scale value, angular resolution, field of view, detector size, and sensitivity degradation due to detector dead area and telescope vignetting), extreme attention must be dedicated to the background minimization. In this respect, key issues are represented by the passive baffling system, which in case of large focal lengths requires particular design assessments, and by the active/passive shielding geometries and materials. In this work, the result of a study of the expected background for a hard X-ray telescope is presented, and its implication on the required sensitivity, together with the possible implementation design concepts for active and passive shielding in the framework of future satellite missions, are discussed.

Keywords: X-ray telescopes, X-ray optics, background

1. INTRODUCTION

The study of the universe above 10–20 keV is still hampered by the absence, up to now, of focusing telescopes for this energy band. This region of the electromagnetic spectrum contains the potential for a dramatic improvement in our understanding of a number of key astrophysical problems which remain still open, such as the origin of the cosmic X-ray background (CXB) in the 20–40 keV where its energy density peaks, or the history of super-massive black holes (SMBH) growth¹. Despite its scientific importance, technological problems have prevented so far the development of suitable hard X-ray telescopes.

The most sensitive experiment flown at these energies, BeppoSAX/PDS², had a flux limit of $\approx 300 \mu\text{Crab}$ at ≈ 30 keV. However, because of its large field of view (FOV $\sim 1.3^\circ$ in diameter) and lack of imaging capabilities, the experiment was limited by high intrinsic background and source confusion. The IBIS imager³ currently operative

Send correspondence to G. Malaguti, E-mail: malaguti@bo.iasf.cnr.it, Telephone: +39 051 6398679

onboard the INTEGRAL satellite, which is based on a coded aperture mask is, on the other hand, capable of only moderate imaging power (angular resolution $\simeq 12'$). Its large FOV ($\sim 30^\circ \times 30^\circ$ at zero response) however, determines a high background level which results in a sensitivity slightly worse than the BeppoSAX/PDS one.

Recent technological advancements in the field of both X-ray mirrors and focal plane detectors, allow for the first time the development of fine imaging, deep sensitivity high energy satellite-borne telescopes for the energy band above 10 keV, some of which have already had a protoflight balloon test⁴. The use of X-ray focusing mirrors very significantly reduces the instrumental background by concentrating the flux into a tiny region (few hundreds of μm) of the detector. However, since many of the key science objectives require very long observations ($10^5 \div 10^6$ s), the residual focal spot area background can eventually dominate the telescope's sensitivity. For these reasons, the evaluation of the expected background and its characterization in terms of cosmic diffuse against particle induced component acquire paramount importance.

At present, different design philosophies have been proposed for the forthcoming hard X-ray focusing telescopes, which are based either on free flyer (HEXIT-SAT¹) or formation flight (Simbol-X⁵, XEUS⁶) mission scenarios. Since the in-flight background is expected to vary according to the mission technical design and orbit choices, dedicated studies are necessary. The present work is aimed at the study of the impact on the limiting sensitivity caused by the background and the other telescope key parameters. The science-driven design concepts and their possible implementations of passive and active shielding in the framework of the forthcoming satellite missions are then presented and discussed.

2. TELESCOPE SENSITIVITY

The minimum detectable flux for a focusing X-ray telescope is given by

$$F_{\min} = n_\sigma \frac{\sqrt{B \cdot A_d}}{\varepsilon \cdot \eta \cdot (1 - \beta) \cdot A_{\text{eff}}^i \cdot \sqrt{N \cdot T \cdot \Delta E}} \quad \text{photons cm}^{-2} \text{ s}^{-1} \text{ keV}^{-1}, \quad (1)$$

where B is the background flux (in counts $\text{cm}^{-2} \text{ s}^{-1} \text{ keV}^{-1}$), A_d is the dimension of the spot area of each mirror module (cm^2), A_{eff}^i is the collection area of a single module weighted by the total mirror reflectivity (cm^2), N is the number of mirror modules, η is the fraction of incoming X-ray photons reflected within A_d , ε is the detector quantum efficiency, β is the fraction of detector dead area (due to the pitch between two adjacent pixels, plus the possible vignetting caused by collimator walls), n_σ is the statistical significance of the detection, T the integration time (in s), and ΔE the energy band (in keV).

The value A_d depends upon the geometrical assembly of the telescope/detector and on the assumed fraction of focused photons, η . For $\eta = 0.5$, then A_d is given by the following relation:

$$A_d = \frac{\pi}{4} [\tan(\text{HPD} \cdot \text{FL})]^2 \quad \text{cm}^2, \quad (2)$$

where HPD is the Half Power Diameter angular resolution, and FL the Focal Length in cm. Equations (1) and (2) show that since large focal lengths implicate large spot areas, with a consequent increase of the intrinsic background counts, the need to optimize the telescope design in terms of sensitivity imply the necessity of trade-offs also in terms of FL and HPD. The latter, moreover, having further importance in avoiding confusion limited deep observations. Figure 1 shows that an angular resolution around $15''$ requires, for $\text{FL} = 8 \div 10$ m, a spatial resolution below $300 \mu\text{m}$, which relax to $\sim 400 \div 500 \mu\text{m}$ for $\text{FL} = 20 \div 30$ m, to sample the point spread function (PSF) with at least two pixels. On the other hand, the possibility to maintain a moderate FL ($\sim 20\text{m}$), by using multi-layer coated mirrors, allows for a field view (FOV) as wide as $\text{FOV} = 15'$ (FWHM diameter). Such a large FOV has fundamental scientific implications as discussed later in section 3.1 and shown in figure 2.

Total reflection occurs for incidence angles below the critical angle, α_c , which is directly proportional to the square root of the reflecting optics material ρ , and inversely proportional to the incoming photon energy, E . The effective area, A_{eff} , of an X-ray mirror telescope, based on Wolter I optics, is approximately given by:

$$A_{\text{eff}} \propto (1 - \xi) \cdot \text{FL}^2 \cdot \alpha_c^2 \cdot R^2 \quad \text{cm}^2, \quad (3)$$

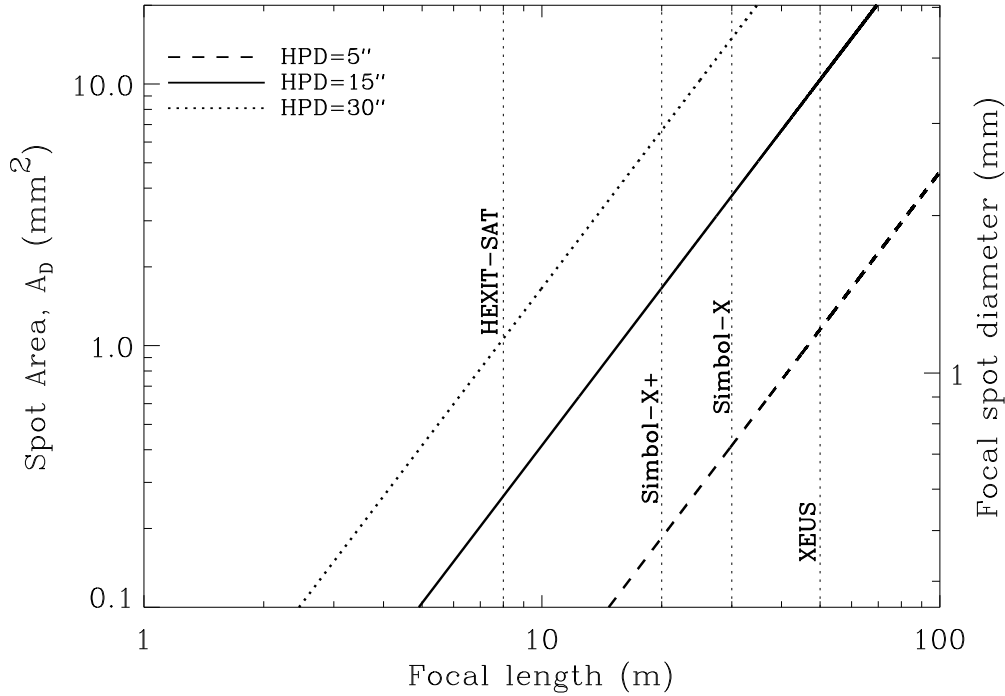


Figure 1. Telescope spot area A_D as a function of the focal length FL for different mission concepts and angular resolutions HPD. The left hand Y axis gives A_D in mm^2 to get a direct evaluation of the associated background variation. The right hand Y axis gives the linear dimension of the focal spot, for a direct comparison with the required detector spatial resolution.

where α_c is the reflection critical (i.e. maximum) angle, R is the reflectivity of the mirrors, and ξ is the telescope area loss due to the vignetting caused by the spider arms or by the finite thickness of the mirror shell walls. For energies $E > 10$ keV the cut-off angle, α_c , becomes very small, thus implying very small effective areas for traditional (FL < 8m) telescopes. For example, even in the case of high density material optics like Platinum ($\rho = 21.4 \text{ g/cm}^3$), the value of α_c at 30 keV is more than five times smaller than at 5 keV (0.15° against 0.8°).

Equation (3) shows that A_{eff} can be increased, with an associated sensitivity improvement, either by having a large focal length, and/or a higher upper threshold value for α_c , which can be attained by using multi-layer mirrors. Conversely, figure 1 shows that a longer FL implies a larger spot area (factor of $\sim 10 - 15$ increase in A_D , if going from FL=8m to FL=30m), and therefore a higher residual background counting rate.

3. BACKGROUND AND SENSITIVITY REQUIREMENTS: THE SIMBOL-X MISSION AS A CASE STUDY

The contribution to the CXB due to highly absorbed (i.e.: Compton-thick) AGN, which are undetected in the canonical 2–10 keV band, is $\approx 50 - 70\%$ of the total. This means that in order to discover significant samples of this class of objects, we need to resolve into discrete sources at least 50% of the 20–40 keV CXB. Using the current AGN CXB synthesis models⁷, this implies a limit sensitivity of $\sim 7 \times 10^{-15} \text{ erg cm}^{-2} \text{ s}^{-1}$ or $\sim 0.75 \mu\text{Crab}$ in the 20–40 keV band, coupled with an angular resolution $\text{HPD} < 15'' \div 20''$ in order to avoid, or minimize to $< 20\%$, confusion problems¹.

The problem of extending soft X-ray capabilities, in terms of sensitivity and angular resolution, also at energies greater than 10–20 keV, was previously tackled for the HEXIT-Sat mission¹, which was specifically

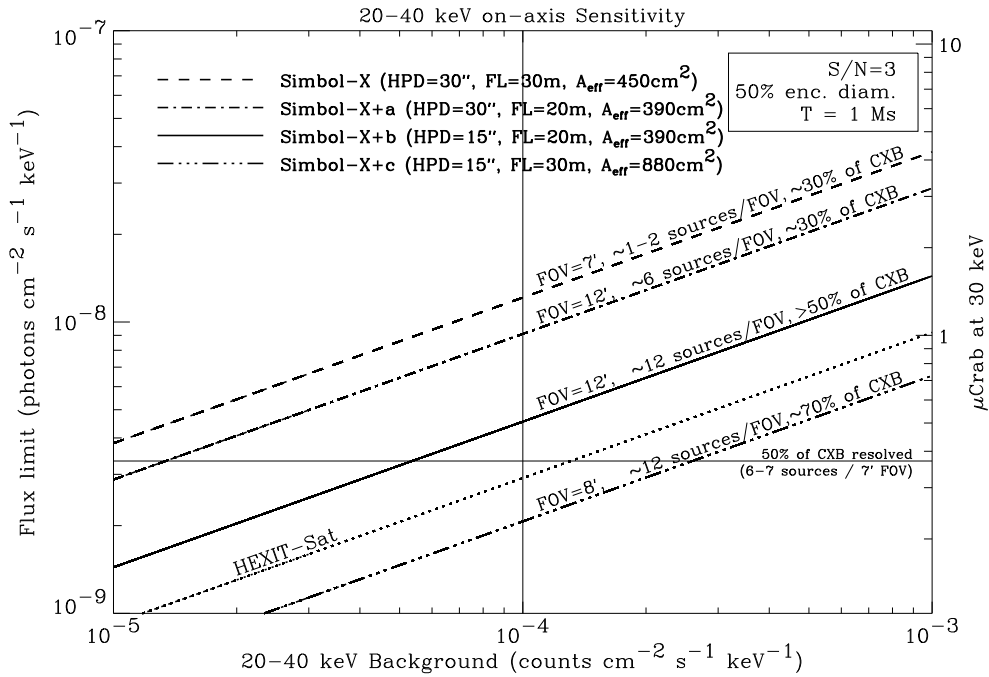


Figure 2. Expected continuum sensitivity in the 20–40 keV band for the current Simbol-X baseline hypothesis compared with the possible mission enhancements (via multi-layer implementation, and mission parameter optimization), as a function of the detector background counting rate. The reported number of sources refer to a 1×10^4 counts $\text{cm}^{-2} \text{s}^{-1} \text{keV}^{-1}$ background, and have been calculated taking into account the increase of the telescope flux limit towards the FOV edge, and considering the effect of the different HPD values on the telescope confusion limit. For comparison, the best telescopes at these energies, INTEGRAL/IBIS and BeppoSAX/PDS provided an angular resolution of 12' (IBIS) and a sensitivity limit of $\sim 300 \mu\text{Crab}$ (PDS).

tailored for this study. This problem has then been addressed by the Simbol-X mission concept study as one of its key scientific objectives. The Simbol-X mission⁵ is an international collaboration led by the CEA/Saclay (France), with groups from Germany and Italy, aiming at a significant leap in the understanding of the sky above 10 keV. The basic Simbol-X principle is to increase the effective area at $E > 10$ keV by means of a long focal length (up to 30 m), while maintaining single-layer Wolter I mirror optics, and allowing maximum optics diameters of the same size as the ones used for XMM-Newton, i.e. ≈ 60 –70 cm. The envisaged mission scenario is to place the detectors and the optics in two separate spacecrafts, exploiting the formation flight configuration concept to be implemented by CNES. The focal plane detector system combines a Si low energy detector, effective up to ~ 20 keV, with a Cd(Zn)Te high energy detector. This hybrid solution allows wide band coverage (~ 0.1 –70 keV), and spectral capabilities ($\Delta E \approx 120$ eV at 6 keV; $\Delta E/E < 3\%$ at 60 keV).

Simbol-X is now at the end of the Phase-0. The selection for the Phase-A is foreseen for autumn 2005, for a beginning of the Phase-A in January 2006. A strong interest has been expressed by the Italian astrophysics community, and by the Italian Space Agency (ASI), for a high level participation to the Simbol-X mission, provided a science-driven optimization of the mission design. The results presented here, specifically oriented to a scientific optimization of the current Simbol-X baseline hypothesis, can be applied, in principle, to any hard X-ray telescope based on focusing optics.

3.1. Sensitivity requirements and evaluation

In its current baseline hypothesis (single-layer optics, FL=30m, HPD=30", FOV=7'), Simbol-X has a sensitivity (see figure 2) $F_{\text{lim}} \approx 1.4 \mu\text{Crab}$ (at 30 keV, in 1 Ms, 3σ , for a background of 1×10^{-4} cts $\text{cm}^{-2} \text{s}^{-1} \text{keV}^{-1}$). This translates into just ~ 2 sources/FOV, resolving about 35% of the CXB at $E > 20$ keV. The feasibility studies

conducted in 2003 for the HEXIT-Sat mission concept¹ have shown that these performances can be enhanced by using multi-layer optics and by optimizing the telescope design. In figure 2 the minimum detectable continuum flux is shown as a function of the expected background, in the 20 – 40 keV energy band. The possible design optimizations choices shown in figure 2, while remaining technically feasible within the Simbol-X mass budget and construction constrains, can allow a sensible improvement of its scientific performance. For the purpose of this study we have focalized on the study of the CXB around 30 keV, and therefore on maximizing the fraction of resolved sources. This can be obtained in several ways: adopting the telescope configuration parameters to reach a deeper sensitivity in a possibly greater FOV, optimizing the mirror shells in order to have the best possible HPD to minimize confusion problems, or by combining the two options.

One of the most interesting mission options is the one labeled as *Simbol-X+b* in figure 2 (continuous line). The key parameters in this option are: FL=20m, HPD=15", and $A_{\text{eff}}=390\text{cm}^2$. The 30% reduction of the focal length (from 30m to 20m, dot-dashed and continuous lines in figure 2), together with the use of multi-layer mirrors, while causing on one side a slight decrease in effective area (see equation 3), would allow a smaller spot area (see equation 2), and a factor ~ 2 (in diameter) greater FOV. In the Simbol-X+b option, these factors are associated to a factor 2 improvement in HPD (from 30" to 15"), and result in a factor ~ 2.5 improvement in sensitivity. Assuming a total detector background of 1×10^4 counts $\text{cm}^{-2} \text{s}^{-1} \text{keV}^{-1}$, this translates in the possibility to resolve into discrete sources more than 50% of the CXB.

On the other hand, the use of the maximum diameter optics ($\sim 70\text{cm}$) which can be hosted within the foreseen spacecraft assembly, coupled with shells capable to reach a 15" HPD, could indeed result feasible even in the presence of the difficulties posed by the high weight. With these optics, and maintaining the 30 m baseline FL, the effective area would be greater than 800cm^{-2} , with a slightly wider FOV (8' in diameter). This would imply a sensitivity of $\sim 0.2\mu\text{Crab}$, which, at this FOV and HPD, would mean to resolve at least 70% of the CXB sources. Moreover, it is important to point out that a further, independent, improvement in the CXB resolution, can be attained by having an even finer HPD, with a consequent minimization of the confusion problems which could arise at these deep sensitivity limits. As a comparison, even because of the absence of imaging capabilities in a 1° FOV (FWHM), BeppoSAX/PDS had already very significant confusion problems with a factor $\sim 50 - 100$ worse sensitivity.

3.2. Background evaluation and active/passive shielding requirements

The background in high energy telescopes is composed by two main components: one is hadron induced, while the second one is directly due to the high energy photons of the cosmic X-ray background. The absolute magnitude of the two components, and the ratio between the two, vary with energy, and depend in principle upon the telescope geometrical set-up (detector material and thickness, field of view, passive shielding design and materials, etc...), the background minimization philosophy (passive and active shielding design, anticoincidence threshold, *good* events characterization and reconstruction, etc...), and the telescope mission scenarios (orbit choice, spacecraft configuration, ...).

The popularity of CdZnTe (CZT) as focal plane detector material for hard X-ray focusing telescopes has constantly increased in recent years, as it has been proposed for several high energy mission projects or ideas: HEFT⁸, NuSTAR⁹, Constellation-X/HXT¹⁰, XEUS⁶, InFOCUS¹¹, Simbol-X⁵, HEXIT-SAT¹. The commonality among the current designs is the placement of the CZT inside deep (active and/or passive) anticoincidence wells. However, these types of instruments have still to be considered to be in their pioneering phase, since on-orbit measurements, performed with focussing CZT telescopes above 10-20 keV, are still lacking.

Recent balloon experiments^{11,12}, based on an actively (organic plus inorganic) and passively shielded CZT detectors, have measured a background level which varies, depending on the detector configuration and aperture angle. These measurements are reported in figure 3, superimposed to the expected CXB flux contribution¹³, as a function of collimator aperture. The InFOCUS measurement¹¹ refers to the July 2001 flight performed with a 2mm thick CZT detector which had a shield opening angle of 8.1° . The other balloon result¹² shown in figure 3 is instead the extrapolation down to a 5° aperture of a measurement performed with a 2mm thick CZT detector having a very wide aperture angle ($\sim 40^\circ$). These two balloon measurements have been normalized to a cosmic environment, assuming a factor ~ 3 reduction due to residual (3 g/cm^{-2} at balloon altitudes) atmospheric absorption. The point at 2° aperture is the result of the MonteCarlo evaluation performed for the

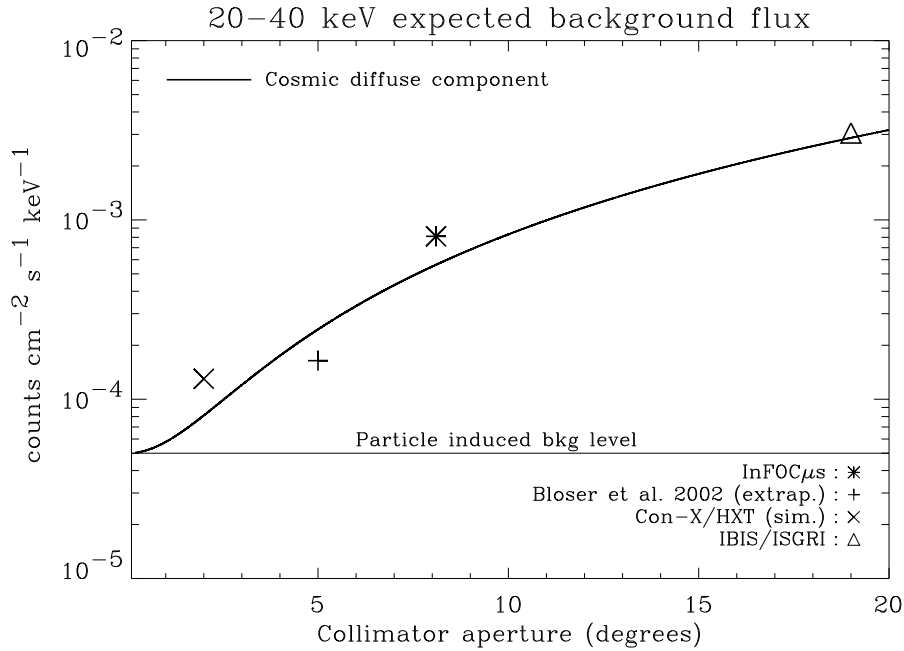


Figure 3. Expected background flux in the 20-40 keV band as a function of the collimator aperture. The continuous line represents the diffuse CXB convolved with the collimator response, while the thin horizontal line shows the particle induced background level re-normalized from BeppoSAX/PDS. The Bloser et al. (2002) point is an extrapolation from a measurement performed with a $\sim 1600\text{cm}^2$ aperture, while the Con-X/HXT point refers to a simulation results (see text). Already at narrow aperture angles, the expected/measured spectrum is dominated by the diffuse component is expected to dominate, and the requirement to have a background $\leq 1 \times 10^{-4}$ counts $\text{cm}^{-2} \text{s}^{-1} \text{keV}^{-1}$, poses a limit of $\simeq 3^\circ$ (in diameter) to the collimator aperture angle.

Constellation-X/HXT instrument in the case of a L2 orbit scenario¹⁴. Finally, the point at 19° corresponds to the background measured by the 2mm thick CdTe ISGRI detector onboard the IBIS telescope³.

The PDS detector² onboard the BeppoSAX satellite, based on NaI-CsI phoswich with passive ($\sim 1.3^\circ$) and active (CsI+plastic) shields, has measured a particle induced background level which, scaled to a 2 mm detector thickness, is equal to $\sim 5 \times 10^{-5}$ cts $\text{cm}^{-2} \text{s}^{-1} \text{keV}^{-1}$. This value, shown as the horizontal line in figure 3, can be used as a reference for the hadronic component, to which one has to sum the contribution of the CXB component to get the total expected background.

Figure 3 shows that already for very small collimator aperture angles, the measured/expected background at 20-40 keV is dominated by the diffuse component. In fact, the requirement to keep the background $\leq 10^{-4}$ counts $\text{cm}^{-2} \text{s}^{-1} \text{keV}^{-1}$ implies a collimator aperture angle $< 3^\circ$ (in diameter). It is important to remind that for this evaluation we have assumed to reject all the possible fluorescence line photons contributions from the passive shielding material itself. This issue will be addressed in section 4, where the possible technical implementations are presented and discussed. The background evaluation shown in Figure 3 has been scaled from balloon and satellite experiments in which the CZT detector was actively and passively shielded. The passive shielding was done by means of a graded (Pb-Sn-Cu) collimator. The active shielding included either a BGO (Constellation-X/HXT, IBIS/ISGRI) or a CsI (InFOCμS) on the rear of the detection plane, while only in one case¹² the possibility to use only plastic has been taken into consideration.

As pointed out in the Constellation-X/HXT simulation report¹⁴, a thick active veto based upon inorganic detector could determine an "overshielding" of the particle induced component, with a consequent increase of the secondary (via isotope activation) emission. For the project under study, however, the passive and active shield design can follow a slightly different philosophy. In fact, given the low, $\sim 80 - 100$ keV, upper energy

Table 1. Design concept key parameters for having a maximum collimator aperture of 3° (corresponding to $\approx 5 \div 10 \times 10^{-5}$ cts $\text{cm}^{-2} \text{s}^{-1} \text{keV}^{-1}$ in the 20-40 keV band. The evaluations refer to the Simbol-X mission (baseline hypothesis, and Simbol-X+b option), and HEXIT-Sat. A simple geometry has been assumed, taking into account only the collimator walls and the covering determined by the optics structure. A detector-collimator separation $s = 3\text{cm}$ has been used (see text and figure 4).

Telescope	FOV (FWHM)	Focal Length (m)	Mirror optics		Collimator height (cm)	
			Diam. (cm)	Subt. angle (deg)	3° apert.	compl. shield
Simbol-X	$7'$	30	60	1.2	167.3	605.4
Simbol-X+b	$12'$	20	70	2.0	148.5	370.9
HEXIT-Sat	$17'$	8	30	2.2	110.7	265.5

threshold, an active/passive shielding system based upon plastic (or inorganic scintillator, but with a thickness significantly smaller than what used for detectors operating in the hundreds of keV region) coupled with a graded collimator can be feasible. Thus, a thinner BGO (or CsI), or a complete replacement of the inorganic crystal with plastic would significantly decrease the activation components, due to radioactive isotopes, which are known to contaminate the background spectrum in the tens of keV region.

3.3. Telescope design concepts

Figure 3 shows that the photon diffused background component dominates above a few degrees collimator aperture, and that in order to meet the required limit of a 1×10^{-4} counts $\text{cm}^{-2} \text{s}^{-1} \text{keV}^{-1}$ background, the collimator aperture must be smaller than $2^\circ - 3^\circ$. On the other hand, given the structure of the focal plane detector and the further shielding due to the optics, the FOV defined by the collimator is not the only parameter to determine the aperture of the focal plane detector to the diffuse background. In fact, in a simple well-type configuration (see also figure 5), the height, H , of the collimator walls, necessary to reach a limiting collimator FOV is given by:

$$H = \frac{FL \cdot \tan\left(\frac{\gamma}{2}\right) + s}{\tan\left(\frac{\phi}{2} + \frac{\delta}{2}\right)}, \quad (4)$$

where:

- ϕ : collimator FOV (FWHM) limit for background minimization;
- s : separation between detector and collimator walls;
- δ : angle subtended by the optics structure at the detector;
- γ : maximum incidence angle for the most external shell;
- α_c : optics critical angle.

The photons which impinge on the most external shell with an angle γ , will be reflected towards the detector with an angle $\theta = 4\alpha_c - \gamma$. Therefore, in order to have a detector *opening angle* large enough to avoid the possible vignetting caused by the collimator walls, the value of s must be $s > H \tan(4\alpha_c - \gamma)$ (see figure 4 and figure 5).

In order to quantify the requirements in terms of collimator walls height, imposed by having a narrow detector aperture, we have taken the Simbol-X mission as a case study, and compared its current baseline hypothesis with an improvement option, which is referred as ‘‘Simbol-X+b’’ in figure 2. The results are shown in table 1. For this calculation we have assumed a simple geometry, taking into account only the collimator walls and the covering determined by the optics structure. The possibility to place a circular shielding structure around the optics would result in a further reduction of the collimator angle, or, for a given detector aperture, in a shorter collimator walls height (see section 4). In the case of Simbol-X the requirement of a 3° collimator aperture translates into a collimator wall height of about 1.7m, slightly higher than what needed for HEXIT-Sat because of its shorter FL. In the Simbol-X+b option, the shorter FL allows for significantly shorter collimator walls also in the case of an even narrower collimator aperture.

The values reported in table 1 have been calculated for a detector-collimator separation, $s = 3\text{cm}$. A non-zero value of s is necessary to avoid vignetting caused by the collimator itself. Indeed, if, on one side, the detector must be shielded against unwanted background photons, the shielding assembly, on the other hand, must not

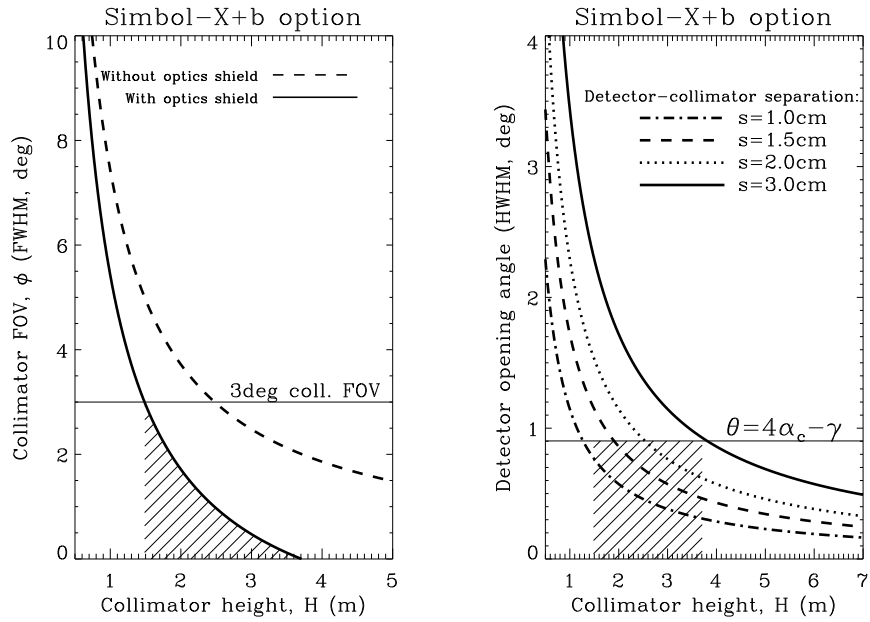


Figure 4. Analysis of the possible trade-offs between collimator FOV (ϕ), collimator height (H), detector opening angle, detector-collimator separation (s), and maximum photon incidence angle on the detector ($4\alpha_c - \gamma$, see text and equation 4), for the Simbol-X+b (FL=20m, FOV=12') mission concept. *Left panel:* Collimator acceptance angle (FWHM FOV) as a function of collimator wall height. The two curves indicate the collimator aperture, with (continuous curve), and without (dashed) taking into account the screening contribution of the optics structure/spacecraft (in the conservative hypothesis of no circular baffling around the optics). *Right panel:* Detector opening angle as a function of collimator walls height, for different detector-collimator separation values (s). Superimposed is the horizontal line corresponding to the maximum photon incidence angle on the detector. The shaded areas in both panels indicate the parameter space allowed in order to have a collimator FOV $\phi \leq 3^\circ$ (left panel), while avoiding vignetting of the focused photons by the collimator walls (right panel).

stop photons coming from within the telescope field of view. This can be obtained by separating the collimator walls from the active detector by a distance, s . In this way, the angular response of the detector will have the canonical shape of a collimated instrument, but with a plateau in the centre. By accurately choosing the combination between collimator height and detector-walls separation, the angular dimension of this plateau (i.e. the detector opening angle) will avoid the vignetting of the focussed X-rays. Figure 4 shows an example of the trade-off analysis between the three relevant parameters: collimator aperture angle, collimator walls height, and detector-collimator separation for the Simbol-X+b (FL=20m, FOV=12') mission concept.

The left panel shows the collimator acceptance angle (FWHM FOV) as a function of collimator wall height. The two curves indicate the collimator aperture with (continuous curve) and without (dashed) subtracting the angle subtended at the detector by the optics structure/spacecraft (in the conservative hypothesis of no circular baffling around the optics). The right panel of figure 4 shows the detector opening angle as a function of collimator wall height, for different detector-collimator separation values (s). Superimposed is the horizontal line corresponding to the maximum photon incidence angle on the detector. The shaded areas in both panels indicate the parameter space allowed in order to have a collimator FOV $\phi \leq 3^\circ$ (left panel), while avoiding vignetting of the focused photons by the collimator walls (right panel). Even in the case of a complete shielding scenario, in the Simbol-X+b configuration the vignetting would be avoided by having a collimator-detector distance $s = 3$ cm.

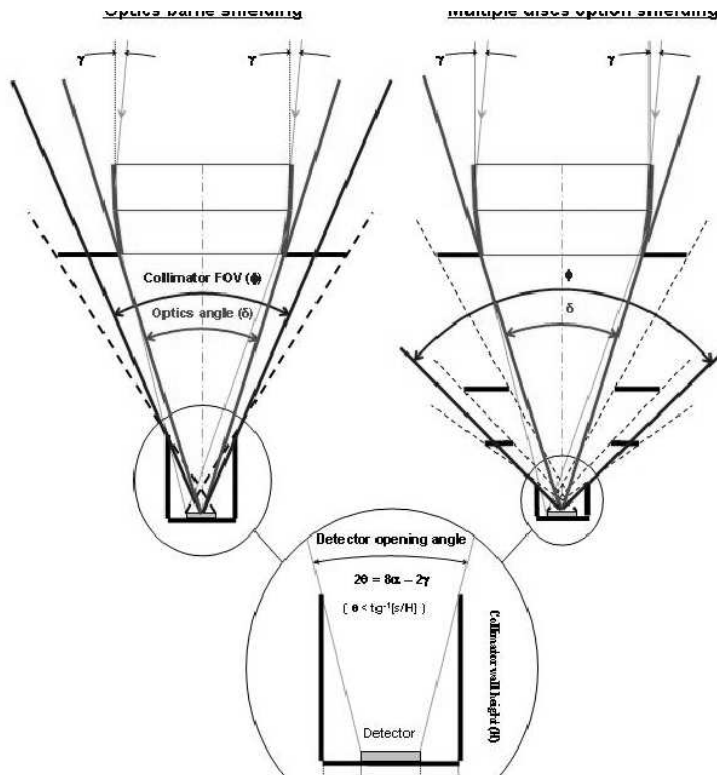


Figure 5. Detector-optics passive shielding concepts: γ = maximum incidence angle for the most external shell; ϕ = collimator FOV (FWHM); δ = angle subtended by the optics at the detector. *Top left panel:* Simple collimator plus optics baffling. *Top right panel:* Shorter collimator coupled with multiple discs structure plus optics baffling. *Bottom panel:* In order to avoid vignetting by the collimator walls, the choice of s (detector-collimator separation) and H (detector walls height) must allow a detector opening angle greater than the maximum focused photon incidence angle on the detector.

4. DESIGN OPTIMIZATION AND IMPLEMENTATION STUDIES

The scientific requirement of having a narrow field of view for the focal plane detector can be met by means of a number of possible configuration designs for the shielding assembly. The technical approach can be divided into two separate solution philosophies which are shown in figure 5: (a) A simple tube-shaped shield (top left panel of figure 5); or (b) a shorter, tube-shaped, passive shield, coupled with concentric and coplanar discs, placed at different heights above the detector (top right panel). The zoomed inset of figure 5 clearly shows how the necessity (which has been quantified in details in figure 4 and table 1) to avoid vignetting by the collimator implies a careful trade-off analysis between H (collimator height), s (detector-collimator separation), δ (the angle subtended by the optics at the detector, α_C , and the telescope FOV. Both options can then be completed with the addition of a disc-shaped structure around the optics (or optics spacecraft, in the formation flight scenario) to achieve a further shielding without increasing the height of the collimator walls.

Solution (a) is naturally feasible for any telescope/detector configuration. Solution (b), on the other hand, can be implemented in the HEXIT-Sat scenario, using the telescope structure itself, while for a formation flight configuration, the use of an extendible bench, in a concept similar to what proposed for sun shielding of the XEUS gratings¹⁵ (in case of their implementation), is feasible.

Within the activity of a pre-feasibility study performed with LABEN/Alenia-Spazio, in the framework of a project financed by ASI, a detailed technical study for a hard X-rays telescope meeting the scientific requirements outlined in section 1, has been carried out. The key aims of the project activity have been the following: (a) definition of the general configuration of the proposed telescope (detection plane, plus active and passive shielding systems); (b) mechanical and thermal design and assessment study of the focal plane; (c) passive shield feasibility

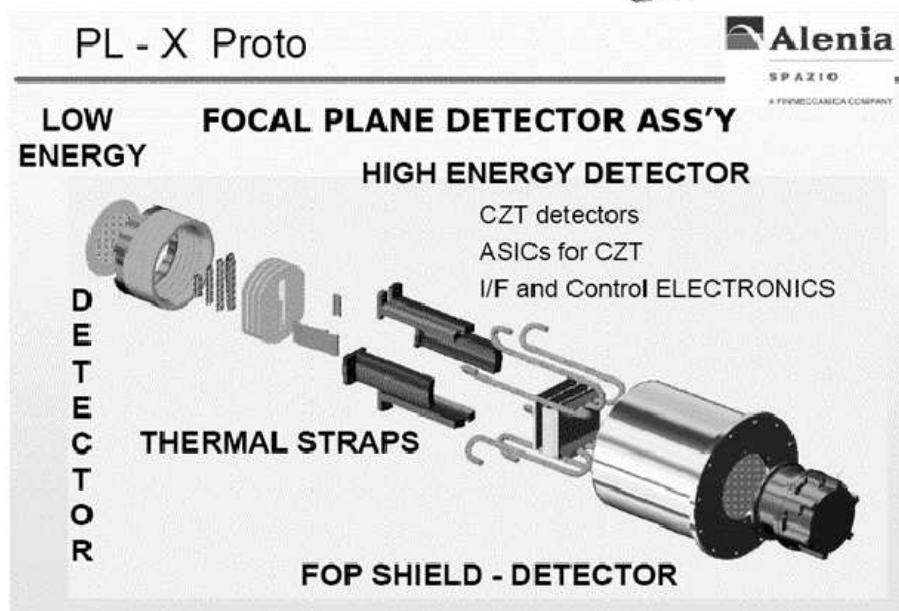
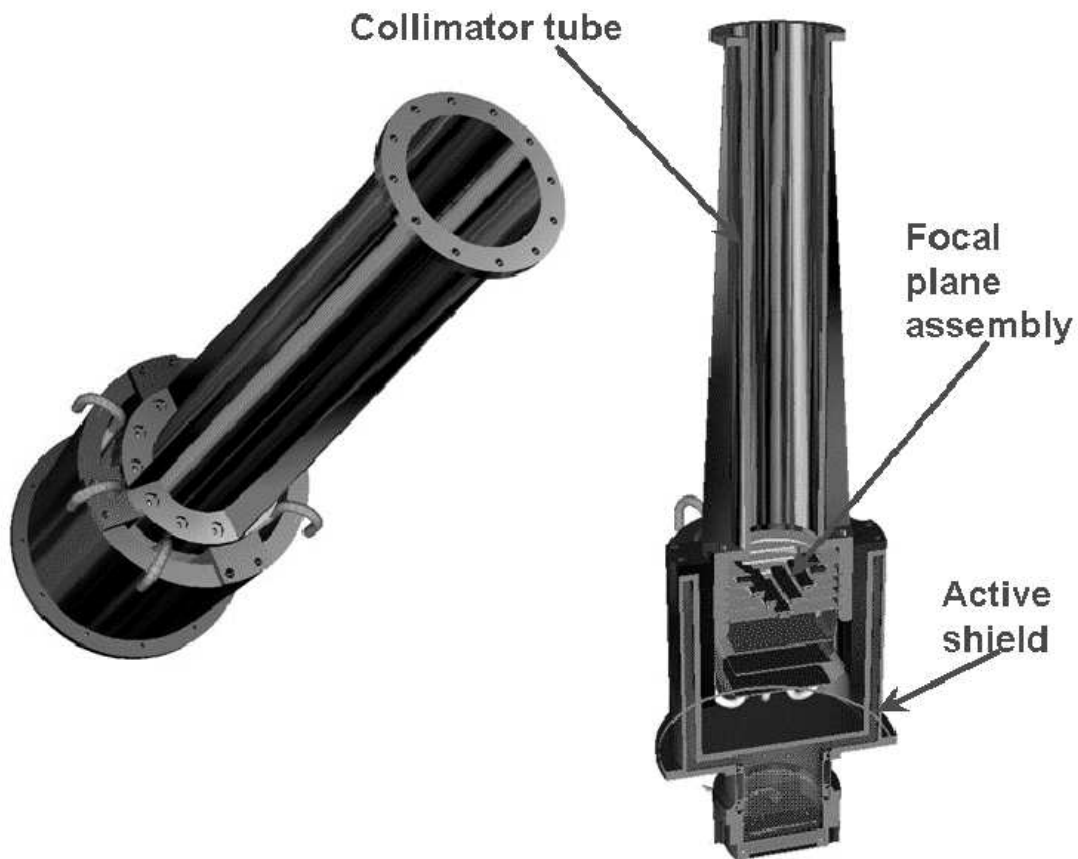


Figure 6. Different views of one of the possible technical implementations which resulted from the pre-feasibility study performed by LABEN/Alenia-Spazio within the framework of a project financed by the Italian Space Agency (ASI). The exploded view (*right and bottom panel*) shows the various subsystems: collimator, focal plane assembly, rear active shield, together with the thermal and electronics interfaces.

study for different possible configurations, with associated design trade-offs and detailed analysis. Figure 6 shows one of the possible technical implementations which resulted from this study. The envisaged telescope concept included: a low energy ($\sim 0.1 - 10$ keV) detector possibly based on Silicon drift detectors; a high energy detector ($\sim 5 - 70$ keV) based on Cd(Zn)Te room-temperature crystals coupled to a dedicated front end electronic ASIC, a rear active shield, and a tube-shaped collimator structure. In addition to the requirement of having a low background, the main design drivers have been: to minimize the length of the thermal paths from the CZT/ASIC assembly to the spacecraft thermal interface; to allow a good distributions of CZT/ASIC power dissipation ($2 \div 3$ W per detector layer), in order to have a uniform temperature across the detection plane; to ensure a modularity design of the high energy detector, to allow for possible non-destructive reworking or detector refurbishment.

Recent measurements¹² have indicated that a well tailored combination of passive and plastic shielding can offer an acceptable background level in tens of keV region. The possibility to avoid inorganic crystals (e.g. CsI, BGO) would have several advantages: plastic is lighter, can be reworked into dedicated shapes without requiring the use of separated ingots, and, most importantly from a scientific point of view, it does not create the activation lines due to radioactive nuclides. In this framework, we have studied the feasibility (see figure 6) of an active shield composed by plastic (e.g. BG-408), surrounded by a high-Z (Tantalum $Z=73$, or Tungsten $Z=74$) graded passive envelope.

Great effort has been dedicated in studying the graded shield configuration in order to minimize the residual background due to $K\alpha$ line fluorescence emission. Four alternative combinations of graded shields have been considered using Tin ($Z=50$) as the first layer, and Copper, Aluminium, and Carbon as additional layer. The use of Carbon as the external layer would minimize the emission also at $E < 8$ keV in order not to contaminate the low energy detector. The thickness of the layers, T_L has been chosen to satisfy the relation $T_L > \mu(E_F)^{-1}$, where $\mu(E_F)$ is the attenuation coefficient at the highest fluorescent energy, E_F , of the neighbouring layer. The total thickness of the various configurations is always below 1.4mm, also in the case of using Carbon which, having a low μ requires the largest thickness.

Further studies are programmed in order to realize, test and calibrate prototypes of both the focal plane detector assembly and the multi-layer optics. In parallel, a dedicated activity is ongoing in order to identify the critical telescope design issues to be addressed to improve the current mission baseline hypotheses.

5. CONCLUSIONS

A detailed study of the sensitivity for a hard X-ray focussing telescope has been carried out. In addition to the already known requirements of a low particle induced background and a fine HPD to minimize confusion problems, the importance to shield against the diffuse background has emerged. The background diffuse component is expected to dominate for aperture angles greater than a few degrees, and the sensitivity requirements impose a maximum collimator aperture of 3° (diameter, FWHM), in order to maintain the background below 1×10^{-4} counts $\text{cm}^{-2} \text{s}^{-1} \text{keV}^{-1}$ at ≈ 30 keV.

The Simbol-X mission has been taken as a case study, and different options, still compatible with the mission mass and dimension budget constraints, have been envisaged which would allow an improvement of the scientific performance with respect to the present baseline hypothesis, having as a key science objective the study of the CXB in the region where it peaks ($20 - 40$ keV). The improvements can be attained mainly by decreasing the FL (30m to 20m) and improving the HPD ($30''$ to $15''$), with a simultaneous increase of the FOV ($7'$ to $12'$) by means of multi-layer implementation.

The possible telescope-collimator-detector configurations have been investigated in terms of parameters optimization. The collimator height necessary to maintain the detector aperture below 3° has been calculated taking into account the additional shielding offered by the optics. A collimator height $H \sim 1.5\text{m}$ would ensure the required 3° aperture. A narrower collimator aperture would need either higher collimator walls, or a disc-shaped shield structure around the optics to increase the covering angle.

A trade-off study between collimator walls height and detector-collimator separation has been carried out and the feasibility to avoid vignetting has been demonstrated also for the smallest (i.e. complete shielding) collimator aperture angles, by means of an acceptable collimator-detector separation $s \simeq 3\text{cm}$.

The result of a feasibility study of a focal plane assembly coupled to an active and passive shielding design concept has been presented.

ACKNOWLEDGMENTS

This work has been financed by the Italian Space Agency (contract I/014/04/0). The use of the facilities of LABEN/Alenia-Spazio is kindly acknowledged. We thank Prof. O. Citterio and Prof G.C. Perola for extensive and extremely fruitful discussions.

6. REFERENCES

1. Fiore, F., et al. 2004, *HEXIT-Sat: a mission concept for X-ray grazing incidence telescopes from 0.5 to 70 keV*, Proc. SPIE, Vol. 5488, p. 933-943
2. Frontera F., et al 1997, *The high energy instrument PDS on-board the BeppoSAX X-ray astronomy satellite*, A&A Supplement series, Vol. 122, p. 357-369
3. Ubertini, P., et al. 2003, *IBIS: The Imager on-board INTEGRAL*, A&A, Vol. 411, p. L131-L139
4. Ramsey, B., et al. 2002, *First images from HERO, a hard X-ray focusing telescope*, ApJ, Vol. 568, p. 432-435
5. Ferrando, P., et al. 2004, *SIMBOL-X: a new-generation hard x-ray telescope*, Proc. SPIE, Vol. 5168, p. 65-76
6. Parmar, A., et al. 2004, *Science with XEUS: the X-Ray Evolving Universe Spectroscopy mission*, Proc. SPIE, Vol. 5488, p. 388-393
7. Comastri et al. 1995, *The contribution of AGNs to the X-ray background*, A&A, Vol. 296, p. 1
8. Harrison, F., et al. 2004, *Development of the High-Energy Focusing Telescope (HEFT) Balloon Experiment*, Proc. SPIE, Vol. 4012, p. 693-699
9. Harrison, F. 2004, *Nuclear Spectroscopic Telescope Array (NuSTAR) mission: Imaging the Hard X-ray Sky*, American Astronomical Society, HEAD meeting #8, #41.05
10. Tumer, T., et al. 2004, *Test results of preliminary CdZnTe pixel detectors for possible application to HXT on the Constellation-X mission*, Proc. SPIE, Vol. 5165, p. 548-553
11. Baumgartner, W. H., et al. 2003, *InFOCuS hard x-ray telescope: pixellated CZT detector/shield performance and flight results*, Proc. SPIE, Vol. 4851, p. 945-956
12. Bloser, P.F., et al. 2002, *Balloon flight background measurement with actively-shielded planar and imaging CZT detectors*, Proc. SPIE Vol. 4497, p. 88-99
13. Zombeck, M. 1991, *Handbook of space astronomy and astrophysics*, 2nd ed., CUP, p. 197
14. Armstrong, T.W., et al. 1999, *Initial estimates of radiation backgrounds for the hard X-ray telescope (HXT) on the planned Constellation-X mission*, Report No. SAIC-TN-99015R3
15. Gerlach, L., et al. 2004, *XEUS Concurrent Design Facility*, ESA, CDF-31(A)